ADVANCED THERAPEUTICS
www.advtherap.com

Recombinant Human Epidermal Growth Factor/Quatsome Nanoconjugates: A Robust Topical Delivery System for Complex Wound Healing

Lidia Ferrer-Tasies, Hector Santana, Ingrid Cabrera-Puig, Elisabet González-Mira, Lídia Ballell-Hosa, Carla Castellar-Álvarez, Alba Córdoba, Josep Merlo-Mas, Haydee Gerónimo, Glay Chinea, Viviana Falcón, Evelyn Moreno-Calvo, Jan Skov Pedersen, Jessica Romero, Claudia Navarro-Requena, Calixto Valdés, Miladys Limonta, Jorge Berlanga, Santiago Sala, Eduardo Martínez, Jaume Veciana, and Nora Ventosa**

A multitude of microparticles and nanoparticles is developed to improve the delivery of different small drugs and large biomolecules, which are subject to several hindering biological barriers that limit their optimal biodistribution and therapeutic effects. Here, a soft, reliable, and scalable method based on compressed CO_2 is reported for obtaining nanoconjugates of recombinant human epidermal growth factor and nanovesicles called quatsomes, where the latter consists of cholesterol and cetyltrimethylammonium bromide. These nanoconjugates exhibit appropriate values of the major critical quality attributes of colloidal nanomedicines, such as controlled and narrow nanoscopic particle size distribution (which play important roles in determining their stability), drug loading, drug release, drug protection, targeting ability, and bioactivity. Also, they exhibit a dual action by 1) inbuilt antimicrobial activity preventing infections and 2) promoting regeneration of granulation tissue and re-epithelialization with complete closure of complex wounds. Therefore, such nanoconjugates are a potential nanomedicine for the topical treatment of complex wounds, particularly diabetic foot ulcers and venous leg ulcers.

1. Introduction

Acute and, in particular, chronic wounds are a global health problem. The incidence of non-healing chronic wounds has exponentially increased with the aging of the population together with the resultant comorbidities of diabetes, venous insufficiency, long hospital stays, and associated chronic diseases. It has been estimated that there is a 2% prevalence of chronic wounds in the general population, which is associated with an annual estimated cost of more than US$50 billion, an expenditure that is expected to rise.[1–3] Chronic wounds, such as diabetic foot ulcers (DFUs), venous leg ulcers (VLUs), and pressure ulcers (PUs), can remain open for months to years.[4,5] Such wounds have been characterized to contain elevated proinflammatory cytokines, high protease levels, excessive neutrophils, and senescent cells that fail to respond to

Dr. L. Ferrer-Tasies, Dr. I. Cabrera-Puig, Dr. E. González-Mira, L. Ballell-Hosa, Dr. E. Moreno-Calvo, Prof. J. Veciana, Dr. N. Ventosa
Institut de Ciència de Materials de Barcelona
ICMAB-CSIC/CIBER-BBN
Campus Universitari, Bellaterra 08193, Spain
E-mail: vecianaj@icmab.es; ventosa@icmab.es

The ORCID identification number(s) for the author(s) of this article can be found under https://doi.org/10.1002/adtp.202000260

[+] Present address: Centre for Clinical Vaccinology and Tropical Medicine, The Jenner Institute, Oxford University, Churchill Hospital, Oxford OX3 7LE, UK

DOI: 10.1002/adtp.202000260

Dr. L. Ferrer-Tasies, L. Ballell-Hosa, C. Castellar-Álvarez, Dr. A. Córdoba, J. Merlo-Mas, Dr. S. Sala
Nanomol Technologies S.L.
Campus UAB, Bellaterra 08193, Spain

Dr. H. Santana, H. Gerónimo, G. Chinea, Dr. V. Falcón, Dr. M. Limonta, Prof. J. Berlanga, Dr. E. Martínez
Center for Genetic Engineering and Biotechnology (CIGB)
31st Avenue between 158 and 190 Streets, Cubanacán, Playa, Havana 10600, Cuba

Prof. J. S. Pedersen
Department of Chemistry and Interdisciplinary Nanoscience Center (iNANO)
Aarhus University
Gustav Wieds Vej 14, Aarhus C DK-8000, Denmark

J. Romero, C. Navarro-Requena
Health and Biomedicine Unit
LEITAT Technological Center
C/ de la Innovació, 2, Terrassa, Barcelona 08225, Spain

Dr. C. Valdés
National Institute for Angiology and Vascular Surgery
1551 Calzada del Cerro, Cerro, Havana 12000, Cuba

reparative stimuli.[6] Open wounds leave the wound bed at risk for colonization by opportunistic pathogens, aggravating the patient's situation. Bacterial colonization of wounds is often facilitated by the production of a slimy extracellular matrix, known as biofilm, which is thought to affect up to 80% of chronic wounds. Nearly half of all DFUs are classified as infected, which strongly correlates with amputation and increased mortality.[7] Despite the benefits demonstrated by biomaterial-based treatments in improving small-sized and uncomplicated neuropathic ulcers,[8] finding effective therapies that could reduce amputations in ischemic and complicated forms of neuropathic wounds remains a challenge.[9,10]

Biologics depict a new category of drugs, which have rapidly gained impulse in the past decade due to their high selectivity and potent therapeutic efficacy along with limited side effects.[8] Since discovered by Cohen in 1962, biologic molecules, named epidermal growth factors (EGFs), have attracted intense interest due to the potential applications in various human health care facets, especially aimed at the enhancement of the healing process. The deficiency of EGF is thought to be one of the pathophysiologic fundamentals in complex wounds.[11] EGF has been reported to facilitate wound healing when delivered to the wound site, since this protein can promote angiogenesis and regulate many aspects of cellular activity, including cell migration, proliferation, and extracellular matrix metabolism.[12] The EGF protein binds to the EGF receptor (EGFR), a tyrosine kinase transmembrane protein, which is expressed on most human cell types including those that play critical roles for wound repairs such as fibroblasts, endothelial cells, and keratinocytes.[13] Nevertheless, evidence demonstrates that exogenous EGF is rapidly cleared from the topical application site, probably by protease-driven cleavage due to the rich proteolytic environment found in these wounds,[13] affecting the bioavailability and effectiveness of the plain EGF-based treatments.

In the present work, an innovative nanotherapy based on recombinant human EGF-loaded quatsomes (EGF@Quatsomes) composed of cholesterol and the quaternary ammonium surfactant cetyltrimethylammonium bromide (CTAB) has been developed as potential nanomedicine to treat topically complex wounds such as DFUs. Quatsomes are nanoscopic vesicles with extraordinary colloidal stability, which favors the production of high-quality pharmaceutical formulations. Due to their properties, quatsomes are an attractive platform for the topical treatment of DFUs because they merge two approaches for nanomaterials used in wound healing:[14,15] 1) they are a promising topical delivery carrier for EGF, which improve protein bioavailability and effectiveness and 2) they exhibit intrinsic antimicrobial properties due to their membrane composition.[16] Indeed, quaternary ammonium surfactants (QASs), like CTAB, are widely used as disinfectants, algaecides, preservatives, detergents, and antistatic components.[17,18]

2. Results and Discussion

2.1. Preparation of EGF@Quatsomes Using DELOS-susp Method

New nanoconjugates based on EGF@Quatsomes have been prepared using a compressed fluid-based procedure called DELOS-susp (Depressurization of an Expanded Liquid Organic Solution-suspension). Unlike conventional methods for vesicle production that are multi-step procedures, this green method, based on using compressed CO_2 as a co-solvent, allows the one-step preparation of nanovesicles with controlled size distribution and particle morphology, and high stability. Besides, this manufacturing process is easily scalable, in comparison to other nanovesicle processing techniques, which is another essential requirement for clinical translation.[16,19] By this process, a volumetric expanded organic solution of cholesterol, CTAB, ethanol, and compressed CO_2 was depressurized over a 5×10^{-3} M histidine–HCl aqueous solution (pH 7.0), containing also the recombinant human EGF (rhEGF) protein at the chosen concentrations, following the procedure described in more detail in the Supporting Information. Using all preparations, the same final concentration of membrane components, four different rhEGF bulk concentrations were tested for preparing nanoconjugate suspensions of rhEGF (0, 25, 100, and 200 μg mL^{-1}). No further steps were required for achieving the desired conjugates' structural characteristics or for increasing the loading (information about the compositions used for the preparation of the vesicles and more details about the process are given in the Supporting Information). With this procedure, homogeneous, opalescent colloidal dispersions of EGF@Quatsomes in water with 10% of ethanol (v/v) were obtained (Figure S1, Supporting Information).

To note, the EGF@Quatsomes are topically administered in their liquid form, as an aqueous dispersion of nanovesicles.

2.2. Physicochemical Properties of EGF@Quatsomes

2.2.1. Particle Size, PDI, Zeta Potential, and Morphology

Mean particle sizes, particle size distributions (or polydispersity index (PDI)), and apparent zeta potentials of the EGF@Quatsomes prepared at bench scale were determined with a Zetasizer Nano ZS as described in the Supporting Information. These are major critical quality attributes of colloidal systems, which play an important role in determining their stability, drug loading, drug release, biodistribution, and targeting ability.[20]

Mean vesicle size of EGF@Quatsomes with 25 and 100 μg mL^{-1} of protein and Blank@Quatsomes (same formulation but without rhEGF) was below 200 nm and similar to each other, meaning that the protein concentration does not alter the mean size of the quatsomes (**Table 1**). However, when increasing the protein concentration above 100 μg mL^{-1}, in this case to 200 μg mL^{-1} of rhEGF, although the mean size was maintained in this nanoscale range, a trend towards larger particle size (from 66 to 184 nm) was observed, as shown in Table 1. The PDI and apparent zeta potential were also influenced by the rhEGF concentration in the colloidal systems. When the protein concentration was above 100 μg mL^{-1}, the PDI value also increased, reflecting a major heterogeneity of the dispersion. In contrast, the zeta potential, which represents the electrical charge at the vesicles' surface being also an important parameter that allows correlating with colloidal stability, decreased drastically at the highest tested protein concentration in the EGF@Quatsomes. Nevertheless, very high apparent zeta potential values (above +70 mV) were found with Blank@Quatsomes and also when loaded with

Table 1. Physicochemical characteristics of free rhEGF, Blank@Quatsomes, and EGF@Quatsomes loaded with different rhEGF concentrations prepared with a bench-scale reactor measured after 1 week. Results are shown as mean ± SD, $n = 2$.

Vesicle systems (rhEGF concentration)	Size mean [nm][a)]	Size PDI[b)]	Apparent zeta potential [mV]	EE [%]	Theoretical rhEGF loading [μg mg^{-1}][c)]
Free rhEGF (500 μg mL^{-1})	2.5 ± 0.55[d)]	–	−16 ± 3	–	–
Blank@Quatsomes	66 ± 5	0.27 ± 0.01	103 ± 3	–	–
EGF@Quatsomes (25 μg mL^{-1})	65 ± 1	0.32 ± 0.04	97 ± 4	97 ± 3	4.6
EGF@Quatsomes (100 μg mL^{-1})	68 ± 5	0.29 ± 0.00	82 ± 0	98 ± 1	18.1
EGF@Quatsomes (200 μg mL^{-1})	184 ± 4	0.44 ± 0.03	[e)]	97 ± 5	36.3

[a)] Intensity weighted mean hydrodynamic diameter of a collection of vesicles, measured by DLS; [b)] PDI of the particle size distribution; [c)] Mass of the integrated protein divided by the total mass of membrane components (cholesterol and CTAB) forming the nanovesicles; [d)] Size of the peak corresponding to the distribution by volume (99.8% volume); [e)] Data not reliable.

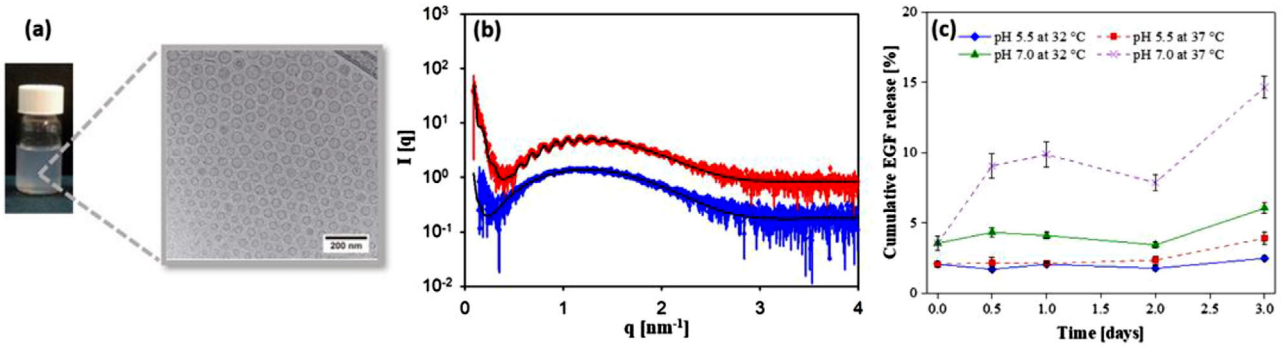

Figure 1. Characterizations of EGF@Quatsomes. Nanoconjugates synthesized by DELOS-susp methodology. a) Macroscopic opalescent appearance and cryo-TEM image of EGF@Quatsomes (rhEGF 100 μg mL^{-1}) suspension. Scale bar 200 nm. b) Experimental SAXS profiles as a function of scattering vector modulus q at room temperature of Blank@Quatsomes, in blue, and EGF@Quatsomes ((rhEGF 100 μg mL^{-1})) loaded dispersions, in red. c) The time-release profile of EGF@Quatsomes (rhEGF 100 μg mL^{-1}) at pH 5.5 (32 °C, blue line, and 37 °C, red dashed line) and pH 7.0 (32 °C, green line, and 37 °C, lilac dashed line). In c, data plotted as mean ± SD (n = 3 per group).

protein concentrations of 25 and 100 μg mL^{-1}, in accordance with the great stability found for these conjugates (Table 1). The entrapment efficiency percentages (EE%) were determined using a combination of ultracentrifugation and rhEGF quantitation by intrinsic fluorescence intensity of tryptophan (Trp) residues (see Methods, Supporting Information, for details). The EE% remained very high (≥97%) for all obtained conjugates regardless of the protein loadings (Table 1). These high values can be rationalized by the negative apparent zeta potential value (near to −16 mV) of free rhEGF and the positive values (near to +103 mV) for Blank@Quatsomes strongly suggesting that the protein should be electrostatically interacting with the quatsomes' membrane (Table 1). Physicochemical stabilities of the EGF@Quatsome systems under storage conditions (refrigerated conditions at 5 ± 3 °C) were also studied after 0, 1, 2, and 3 weeks. The stability was evaluated in EGF@Quatsomes at protein concentrations of 25 and 100 μg mL^{-1} and in the case of 100 μg mL^{-1} EGF@Quatsome system; week 90 was also evaluated to corroborate the high stability over time of this system, which is the one with more integration of rhEGF with good physicochemical properties (Figure S2 inset, Supporting Information). Results of size and PDI were determined to show that these quality attributes remain stable during the storage conditions studied.

The morphology of the conjugates is another important quality attribute for its performance. Therefore, the EGF@Quatsomes were characterized with cryo-transmission electron microscopy (cryo-TEM) depicting the presence of spherical, homogeneous, and unilamellar vesicles (**Figure 1**a; Figure S3, Supporting Information). The effect of rhEGF loading (25–100 μg mL^{-1} final concentration) on the EGF@Quatsomes' morphology was also evaluated. The formulation with 200 μg mL^{-1} of rhEGF was not included due to its instability (vide infra). As shown in Figure S3, Supporting Information, all systems present similar sizes as observed in dynamic light scattering (DLS). On the other hand, small-angle X-ray scattering (SAXS) measurements were performed on Blank@Quatsomes and EGF@Quatsomes (rhEGF 100 μg mL^{-1}) (Figure 1b) to study their homogeneity (see Methods, Supporting Information, for details). This technique can provide unique structural information with the advantage of measuring the average properties of the bulk samples that can be otherwise obviated by using only microscopic techniques such as cryo-TEM or confocal microscopy. The SAXS data for Blank@Quatsomes and EGF@Quatsomes has a broad maximum at large scattering vector moduli q, which originates from the shell–core–shell cross section structure of the vesicles, where the electron density of the hydrocarbon core is lower than that of the buffer and the electron density of the shells is higher than the buffer.[21] The EGF@Quatsome samples display additional extensive high-frequency ripples, which originates from the overall size of the vesicles and a very low size polydispersity.

The corresponding data for Blank@Quatsomes do not show these oscillations, which means that this sample is somewhat more polydisperse. However, an aged sample (20 months) has also been measured and the data (not shown) display the same high-frequency ripples as the EGF@Quatsomes. Additionally, exposing the Blank@Quatsomes sample to ultrasound also results in SAXS with ripples, and this together with the behavior of the aged sample shows that the equilibrium structure of the Blank@Quatsomes sample is also that of very monodisperse vesicles. Since the fresh EGF@Quatsomes sample already is very monodisperse, it is reasonable to conclude that the association of the rhEGF enhances molecular exchange, which brings the system faster into equilibrium.

The SAXS data were fitted with a model of spherical vesicles with a Gaussian number size distribution, where the cross section of the vesicles is a shell–core–shell structure. The model fits the data very well and reproduces the high-frequency ripples for the EGF@Quatsomes confirming a vesicular structure, as observed by cryo-TEM (Figure 1a). According to the modeling, the outer radius for the Blank@Quatsomes and the EGF@Quatsomes was 31 ± 8 and 27.22 ± 0.03 nm, respectively, whereas the membrane thickness for both samples was 4.4 nm. The polydispersity for the Blank@Quatsomes is estimated to be >10%, whereas it is only 2.6% for EGF@Quatsomes. These results are in agreement with the cryo-TEM micrographs (Figure 1a; Figure S3, Supporting Information) and DLS results (Table 1; Figure S2, Supporting Information), when considering that the polydispersities from DLS are usually overestimated.

The release profile of rhEGF from the EGF@Quatsomes with 100 μg mL^{-1} of rhEGF in the dispersant media conditions (EtOH/water 10% v/v, histidine–HCl buffer 5×10^{-3} M at pH 5.5 and 7.0) was investigated through the shaking incubation of the conjugates at 32 and 37 °C and after storage times of 0.5, 1, 2, and 3 days. The released rhEGF was determined by ultracentrifugation followed by ELISA (Figure 1c). No burst release of loaded rhEGF was clearly observed at the beginning of the study at both pH values, neither any rhEGF release was observed for the sample maintained during 3 days at pH 5.5 after incubation at temperatures 32 and 37 °C. However, at pH 7.0 a small rhEGF release was observed that tends to slightly increase as a function of time but remains below 5% after the 3 days at 32 °C. A slightly higher rhEGF release was detected at the same pH after storage at 37 °C, being practically nonrelevant (from 10 to 15%). The presence of the histidine medium in the nanoconjugates' composition could explain this finding. The free histidine amino acid can behave as a competitor of the rhEGF binding to the Quatsomes' surface. As shown above, Quatsomes are highly positive charged as indicated by Z-potential values of +103 mV and +82 mV for the Blank@Quatsomes and the EGF@Quasomes (100 μg mL^{-1}), respectively (Table 1). The net positive charge is indicative of the presence of an excess CTA^+ ion over the negatively charged bromide counter ion. Since histidine is present in the nanoconjugates at 5 mM bulk concentration, and rhEGF at 100 μg mL^{-1} (about 16 μM), this represents about 300 fold higher molar concentration of histidine than rhEGF. The binding of histidine to Quatsomes is likely characterized by a) ionic interactions of the zwitterion groups of the amino acid $[NH_3]^+$ and $[CO_2]^-$ with the Br^- anion and CTA^+ head, respectively, b) the interaction between the imidazole group and the CTA^+ moiety. Similar behavior of some amino acids and their group contributions in aqueous Tetramethylammonium Bromide (TMA) has also been reported,[22] in which the interactions depicted in the aforementioned case (a) are predominant, and the amino acid behaves as a disruptive solute. Taking these findings into account, it can be concluded that at pH 5.5 the protonated side chain would display unfavorable interaction with the CTA^+ cation, and at pH 7.0 the neutral imidazole will have favorable - pi-cation and hydrogen bond interactions with the same group of the Quatsome. Accordingly, at pH 7.0 the histidine amino acid could interfere more in the rhEGF binding to the Quatsomes' surface than at pH 5.5, however, being the impact of this effect on the protein release minimum.

To develop a robust nanomedicine that can progress to the clinical stage, it is essential to attain a complete reproducibility of their physicochemical characteristics, morphology, and drug substance loading among different batch productions, which is called batch-to-batch consistency. Besides, it is very important the use of methodologies that allow nanomedicine production at an industrial scale with suitable and reproducible characteristics, involving a minimum number of steps and equipment and meeting the requirements of the pharmaceutical guidelines and the good manufacturing practices (GMPs). In this regard, the reproducibility under a 40-fold scale-up has been checked to evaluate the potentiality of the DELOS-susp as a robust manufacturing platform for the production of EGF@Quatsomes (rhEGF 100 μg mL^{-1}) from bench scale (obtaining 25 mL of nanoformulation) to pilot-scale (delivering 1 L of nanoformulation). Robustness and reproducibility of the EGF@Quatsomes production by DELOS-susp methodology were evaluated by measuring the mean particle size, PDI, apparent zeta potential, and EE% values (Table S1, Supporting Information) of different batches produced at the different scales, by high-pressure vessels with different volumes (Figure S4, Supporting Information). From the obtained data average, one can see that the standard deviations of the mean particle sizes, apparent zeta potentials, and EE% values are small with a coefficient of variation (CV) of 2.6–11.6% in all cases, indicating a high degree of reproducibility during scale-up of the DELOS-susp method for the EGF@Quatsomes preparation.

2.2.2. Structural Characterization of EGF@Quatsomes

The structure of a nanoconjugate is another important quality attribute for the performance of any drug delivery system. Previously, we demonstrated that the EGF@Quatsomes are spherical unilamellar vesicles (Figure 1a,b). To demonstrate experimentally the localization of rhEGF protein in the conjugates, immuno-transmission electron microscopy (immuno-TEM) images were taken in rhEGF concentrations 25 and 100 μg mL^{-1} (**Figure 2**a). In both concentrations, the microscopy images show the presence of black dots corresponding to colloidal gold nanoparticles (about 15 nm diameter) in the vesicle membranes of the EGF@Quatsomes that are not present in Blank@Quatsomes, confirming the localization of rhEGF anchored to the lipidic membrane of vesicles. Furthermore, immuno-TEM images of EGF@Quatsomes reveal the formation of rhEGF clusters, which were clearly localized with a specific

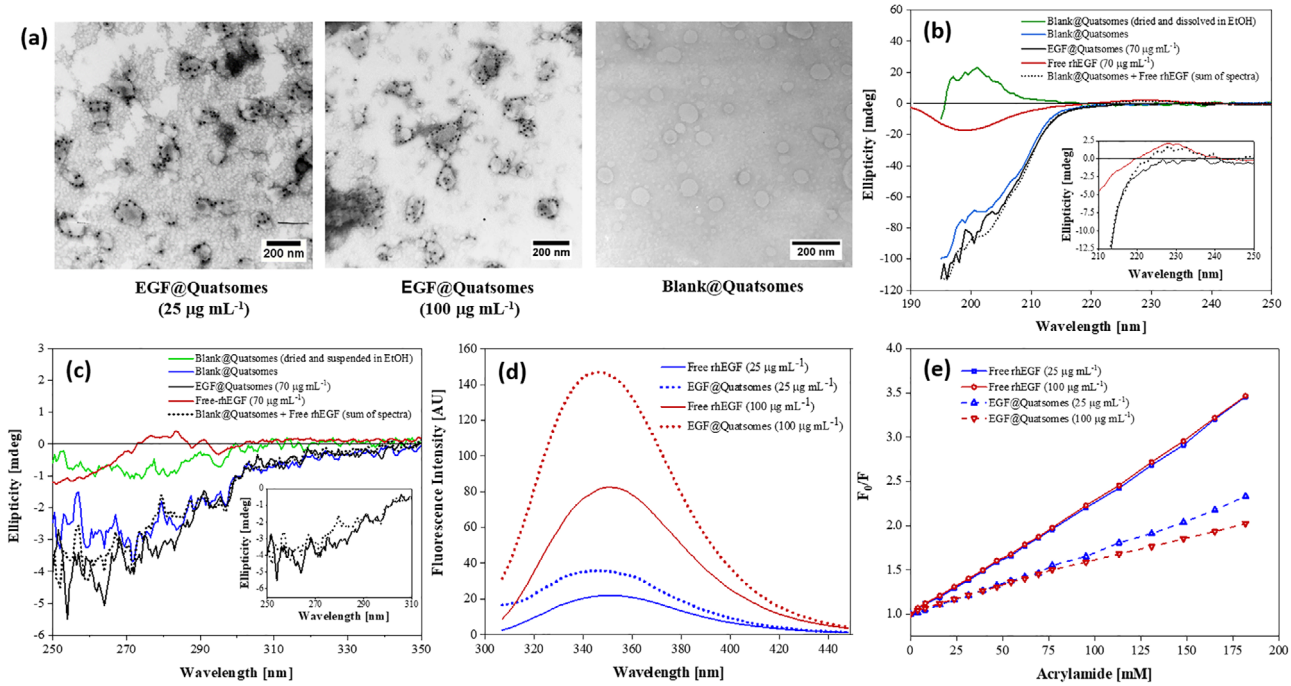

Figure 2. Structure of EGF@Quatsomes. a) Left and middle: Immunoelectron transmission microscopy images showing the localization of rhEGF on the EGF@Quatsomes bilayer with specific monoclonal antibody after detection with secondary rabbit anti-mouse IgG labeled with colloidal gold nanoparticles (15 nm). Right: Immunoelectron transmission image in Blank@Quatsomes showing an absence of rhEGF. b) Far-UV and c) near-UV CD spectra of different samples after dispersant media exchange to water in PD-10 desalting columns: Blank@Quatsomes (blue line), free rhEGF (red line), EGF@Quatsomes (black line), Blank@Quatsomes after dried and resuspended in EtOH (green line), and the sum of spectra of Blank@Quatsomes and free rhEGF (dashed black line). d) Fluorescence emission spectra of free rhEGF at different concentrations (25 and 100 μg mL^{-1}, blue and red solid lines, respectively), and in EGF@Quatsomes at 25 and 100 μg mL^{-1}, blue and red dashed lines, respectively. e) Fluorescence quenching (F_0/F) of the tryptophans present in free rhEGF at 25 and 100 μg mL^{-1}, blue and red squares, respectively, and the nanoconjugates EGF@Quatsomes, at 25 and 100 μg mL^{-1}, blue and red triangles, respectively, in 5×10^{-3} M histidine–HCl buffer at pH 7.0, with acrylamide quencher. In b-e, data plotted as mean (n = 3 per group).

monoclonal antibody. These characteristic rhEGF clusters on the surface of quatsomes indicate the greater ease for the dimerization of the EGFR and potentially it may improve its biological activity.

Since both cholesterol and rhEGF display chiral properties, the structural behavior of quatsomes and rhEGF was further accessed by circular dichroism (CD) spectroscopy. Figure 2b shows the far-UV CD spectra of samples and controls. As a control for quatsomes analysis, Blank@Quatsomes were dried and dissolved with ethanol to generate the sample with equivalent free solution components. This sample generates a positive dichroic band peaking around 200 nm, and a negative band below 195.5 nm. These results are in agreement with the previously reported for free cholesterol solution in cyclohexane and acetonitrile.[23] The self-assembled nanostructured Blank@Quatsomes in water showed large changes in the spectrum as compared with the mixture of free quatsomes components in ethanol, displaying an intense negative dichroic band below 230 nm with higher ellipticity values the spectral range of 195–220 nm. The experimental spectrum of EGF@Quatsomes was further compared with the spectrum resulting from the sum of the individual spectra of the free rhEGF and Blank@Quatsomes. Both spectra overlap fairly well, suggesting no major structural disturbances taking place by the complex formation and the presence of a common secondary structure profile of the free protein and after its integration to quatsomes. However, the positive band around 230 nm observed in the sum of spectra disappeared in the EGF@Quatsomes spectrum (Figure 2b inset). This band is likely associated with the aromatic amino acids (Trp and Tyr) and, possibly, the disulfide bonds of rhEGF. The loss of the 230 nm positive band in EGF@Quatsomes strongly suggests that upon rhEGF binding to quatsomes surface some changes occur in the structural environment of aromatic amino acids of the protein.

Maintaining the secondary protein structure is an important prerequisite to warrant its biological activity. Hence, the secondary structure analysis from far-UV CD spectra for free rhEGF and EGF@Quatsomes yields consistent estimations for these samples, which contain 30–35% of beta-sheet with the same antiparallel right-twisted structure, 10–14% of turn structure, and 51–61% of unordered structures (Table S2, Supporting Information).

Figure 2c shows the near-UV CD spectra (250–350 nm) of the same samples and controls. Blank@Quatsomes dried and dissolved with ethanol showed a negative band in the range 250–295 nm. The spectrum of self-assembled nanostructured Blank@Quatsomes in water also shows negative but more intense bands. The higher intensity is likely due to the restrictions in orientation in the quatsomes bilayer that offers a limited and specific conformational framework for the cholesterol. The

spectrum of rhEGF displayed a negative band around 295 nm and 250–275 nm and a positive band around 275–285 nm. These bands are attributed to the sum of characteristic vibrionic transitions of structurally ordered aromatic residues (Trp and Tyr) and possibly from disulfide bonds as well. Figure 2c inset shows the comparison of the EGF@Quatsomes spectrum to that of the sum of individual spectra for free rhEGF and Blank@Quatsomes. The appreciated differences again indicate the presence of changes in the structure of aromatic amino acids of rhEGF upon binding to quatsomes.

Intrinsic fluorescence of proteins is another property sensitive to changes in their tertiary structure also revealing the polarity of the microenvironment present around its fluorophores, in particular the Trp residues. Thus, the location—and the structural environment—of such residues determine the intensity value and the wavelength of maximum fluorescence emission, which varies from 330 to 355 nm depending on solvent properties, the degree of solvent exposure, and other local interactions. As already mentioned, immuno-TEM (Figure 2a) results suggested that part of the protein should be interacting with the membrane producing its immobilization. Furthermore, CD spectroscopy (Figure 2b,c) suggests that aromatic amino acids in rhEGF are probably interacting with the cationic membrane. The emission spectrum of free rhEGF in the dispersant medium was characterized by an emission maximum at 350–352 nm (Figure 2d; Table S3, Supporting Information) which indicates that Trp residues reside on the protein surface and are in contact with free water. These results are consistent with those previously reported for Trp in free rhEGF by nuclear magnetic resonance spectroscopies.[24] However, when the rhEGF was integrated into quatsome nanovesicles, the maximum emission was shifted to shorter wavelengths (about 346 nm) and an increase of fluorescence intensity, as compared to the free protein, was observed. This indicates that Trp residues are located in a less polar environment when integrated into the quatsome membrane. Information on the rhEGF location was also obtained by quenching experiments with acrylamide that suggests the rhEGF is less accessible to the quencher acrylamide when grafted to quatsome vesicles (Figure 2e; Table S3, Supporting Information). However, in the free rhEGF samples, the Stern–Volmer constants were larger than those of EGF@Quatsomes, consistent with more exposed Trp residues to solvent at all concentration studies. The data are consistent with findings concerning the relative resistance to proteolytic attack and comparative biological activity values of EGF@Quatsomes with respect to the free protein.

2.3. Interaction between rhEGF and Quatsomes

The interaction between rhEGF protein and quatsomes has been thermodynamically characterized through isothermal titration calorimetry (ITC) measurements (see Methods, Supporting Information, for details) since the binding constants and the stoichiometry of the system can be determined from the measurements. rhEGF interactions with quatsomes are expected to be strong enough so that the major part of rhEGF is linked to the quatsomes and therefore protected from the environment, but weak enough to get the rhEGF released from the quatsomes when they come into contact with the EGFR, thus initiating the cellular signaling for wound healing.

The experiments consisted of the titration of different concentrations of rhEGF (placed on the 290 µL syringe) over different concentrations of Blank@Quatsomes (placed on the 1448 µL sample cell). Due to the high sensitivity of the ITC instrument, Blank@Quatsomes were diafiltrated to remove the 10% of ethanol (v/v) present in the formulation (described in Methods, Supporting Information). Moreover, since errors in the concentration estimation would have a direct impact on the stoichiometry, the exact concentration of cholesterol and CTAB in the diafiltrated Blank@Quatsomes was analyzed by HPLC-ELSD (see Methods, Supporting Information). The final concentration was 2.69 mg mL^{-1} for the cholesterol and 2.20 mg mL^{-1} for the CTAB, with an estimated concentration of quatsomes of 3.40×10^{-7} M. Blanks of rhEGF titrated over histidine–HCl 5×10^{-3} M (pH 7.0) buffer medium were also performed.

By use of the AFFINImeter software (www.AFFINImeter.com), raw data obtained from a plot of heat flow versus injection number were transformed to construct a plot of enthalpy change versus molar ratio (Figures S5 and S6, Supporting Information). The blank isotherm obtained by titrating 0.41×10^{-3} M rhEGF over histidine–HCl 5×10^{-3} M buffer medium showed endothermic peaks in a slope-like shape indicating that the protein was dimerized in the syringe (and de-dimerizing upon contact with the lower concentration of rhEGF in the histidine–HCl 5×10^{-3} M buffer) (Figure S6, Supporting Information), and therefore this blank could not be subtracted from the corresponding titration experiments to account for the heat of dilution. However, the blank performed titrating only 0.05×10^{-3} M rhEGF over the buffer did not show de-dimerization, meaning that at low concentrations, the protein is not dimerized (Figure S6, Supporting Information).

The isotherms shown in Figures S5 and S6, Supporting Information, were also fitted using the software AFFINImeter. The stoichiometric approach was employed to create an original stoichiometric binding model in which the de-dimerization of the protein could be included. The designed model comprised two different equilibriums, one corresponding to the rhEGF dedimerization and one corresponding to the rhEGF binding to the quatsomes (Figure S7, Supporting Information). The model described was applied for a global fitting where all the isotherms were simultaneously fitted and from which thermodynamic parameters were calculated (Table S4, Supporting Information). Those isotherms in which no de-dimerization or in which no interaction rhEGF-Blank@Quatsomes (blank experiment) was occurring were fitted only to one (the required) equilibrium. The affinity constant and the enthalpy change of the two equilibriums were assumed to be equal for all the experiments and were linked and fitted together. Global fitting is particularly useful for the analysis of this kind of complex interactions that involve the presence of more than one equilibrium and in which isotherms share some fitting parameters. By this global fitting, the number of proteins binding per Blank@Quatsome surface was found to be 70 ± 20 at the tested conditions (Table S4, Supporting Information). As shown in Table S4, Supporting Information, the rhEGF interaction with the Blank@Quatsomes is an exothermic reaction. It was expected to be an electrostatic interaction, since at pH 7.0 the rhEGF is negatively charged, and the Blank@Quatsomes

are positively charged, and for charged proteins, electrostatic attraction is predominant, as described in the literature.[25] However, electrostatic bindings are characterized by small ΔH values; a typical example is the binding of heparan sulfate to charged vesicles with $\Delta H = -2 \times 10^3$ cal mol^{-1}.[25] In our studied system, the ΔH of this first equilibrium was high, $\Delta H = (-6.69 \pm 0.05) \times 10^4$ cal mol^{-1}, indicating that another kind of binding was acting together with the electrostatic binding. This extra energy registered could correspond to hydrogen bonding between the head of the CTAB molecules and the rhEGF protein[26] or a reorganization of the rhEGF structure upon contact with the Blank@Quatsomes. As was previously evidenced by both CD and intrinsic Trp fluorescence, aromatic amino acids are probably implicated in rhEGF binding to the quatsome surface. Then, extra energy could also come from π-cation and π-stacking interactions of aromatic amino acids (Trp and Tyr) in rhEGF with CTAB and cholesterol, respectively.

Considering all the experiments performed, it seems that the rhEGF gets in contact with the Blank@Quatsomes attracted by the electrostatic forces and binds to the Blank@Quatsomes with electrostatic bindings. Also, hydrogen bonding or protein reorganization occurs at this stage, releasing energy. Importantly, the results show that the interaction has a binding constant K_a equal to $(5.00 \pm 0.05) \times 10^5$ M^{-1}, therefore a dissociation constant K_d ($= K_a^{-1}$) of 2×10^{-6} M (Table S4, Supporting Information). The dissociation constant of the rhEGF and the EGFR is well described in the literature and is of the order of 1×10^{-9} M.[27] Importantly, the determined value indicates that the rhEGF has a stronger affinity for its receptor than for the Blank@Quatsomes, which makes the quatsomes appropriate delivery systems, desirable for the transportation of the protein since the interaction between the rhEGF and the quatsomes do not compromise thermodynamically the interaction of the protein with its receptor.

2.4. In Vitro Protein-Specific Bioactivity of EGF@Quatsomes

The manufacturing process used to prepare the nanoconjugates must not impair the protein bioactivity with the consequent loss of its function in the site of action. Therefore, the bioactivity of the EGF@Quatsomes was determined by the ability of the samples to induce cell proliferation in 3T3 A31 mouse fibroblast cells, since this cell line shows overexpression of EGF receptor.[28] First, to determine the cytotoxicity and cell biocompatibility of the quatsomes, a dose–response curve was assayed using the same cell line as for the cell proliferation test. The viability assay at 24 h of incubation time revealed that cationic nanoconjugates exhibited dose-dependent toxicity. When cells were exposed to EGF@Quatsomes and Blank@Quatsomes with a CTAB surfactant concentration higher than 6.7 μg mL^{-1}, cell viability was reduced to about 40%. However, being Quatsomes diluted and cells exposed to surfactant concentrations from 3.35 to 0.8375 μg mL^{-1}, Blank@Quatsomes did not present any cytotoxic effect. Besides EGF@Quatsomes exhibited statistically significant increased cell proliferation activity (about 50% increased) as compared to the Blank@Quatsomes group (Figure S8 and Table S5, Supporting Information). Taking into account this finding, the minimum dilution of quatsomes valid to perform a cell proliferation assay and study their bioactivity must be 1/400-fold, since at this dilution quatsomes contains a CTAB concentration of 6.7 μg mL^{-1} (the maximal non-cytotoxic concentration).

To compare the specific bioactivity of the protein at different EGF@Quatsomes formulations, the specific activity of the samples was calculated by dividing the absolute biological activity by the protein concentration of each sample. Blank@Quatsomes were also included as a control in these assays and no cell proliferation increase was observed. A worth noticing point of these experiments was that the rhEGF bioactivity was not only preserved after EGF@Quatsomes preparation by DELOS-susp methodology but also increased (**Figure 3**a). The half-maximal effective dose (ED_{50}) of EGF@Quatsomes and free rhEGF towards fibroblast cell line lines were in the ranges 1.27–1.40 and 2.70–3.06 ng mL^{-1}, respectively. This increase was at least twice the potency for EGF@Quatsomes, compared to the free biomolecule at the same bulk concentration. As expected, cell proliferation shows dose–response within the range of tested concentrations for both free rhEGF and EGF@Quatsomes (Figure S9, Supporting Information). At low rhEGF concentrations (0.625–5.0 ng mL^{-1}), EGF@Quatsomes also have statistically significantly higher cell proliferation activity than free rhEGF at the same bulk concentration (Table S7, Supporting Information). As discussed in a previous section, the activity increase could be related to the immobilization of the protein in the vesicle membrane with probably a "site-specific" orientation of the active protein region towards the surrounding media, which is favorable for interaction with the EGFR. It is well-known that the EGFR is organized in small clusters of 150 nm average diameter on the cells' plasma membrane.[29] This surface matched well with that of the EGF@Quatsomes with an average diameter of 50–70 nm (Figure 1a,b). Additionally, the presentation of the immobilized ligands attached to the quatsome membrane would induce a nanometer-scale clustering of the ligand. This would favor the multimerization of the receptor; since two receptors that bind to ligands immobilized on the same quatsomes would be nearby, favoring dimerization-dependent signaling (Figure 3b).

2.5. In Vitro Resistance of EGF@Quatsomes to Proteases

Chronic wounds, such as DFUs, present a proteolytic environment that can affect the bioavailability of protein-based drugs used during treatments. Therefore, the protective properties of EGF@Quatsomes were evaluated through their capacity of preserving the rhEGF stability and bioactivity in the presence of proteases. In this study, chymotrypsin was selected as a protease model because it has many cutting sites in the rhEGF sequence, and its rhEGF proteolysis was sensitive to the ELISA assay. The results showed that at the same rhEGF bulk concentration, all EGF@Quatsomes presented increased stability against chymotrypsin when compared with the free protein (Figure 3c). As expected, for the same kind of sample, with higher rhEGF concentration, higher proteolysis was observed, probably because saturation conditions were not reached. Thus, during the first 3 h, the amount of protein decreases in all cases, however, for the EGF@Quatsomes formulations the decrease was much smaller. Between 3 and 24 h of incubation, the protein contents remained practically constant near to 20% for free rhEGF at 25 μg mL^{-1} and lower than 5% for free rhEGF at

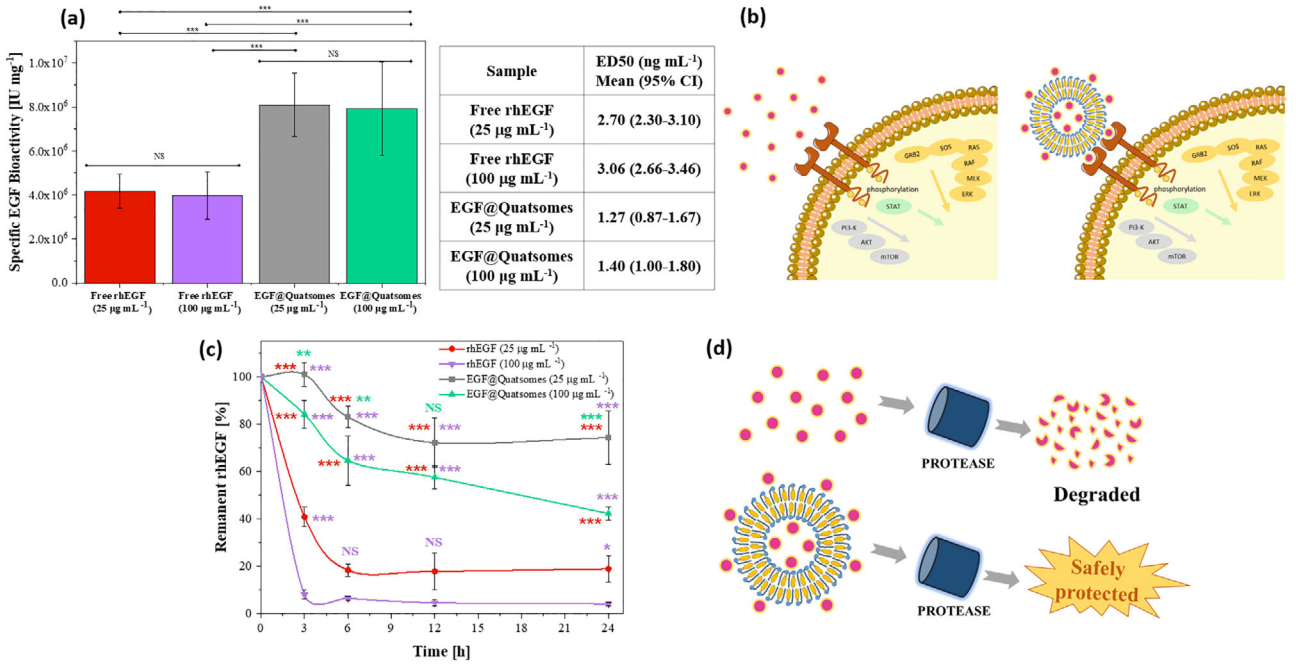

Sample	ED50 (ng mL^{-1}) Mean (95% CI)
Free rhEGF (25 µg mL^{-1})	2.70 (2.30-3.10)
Free rhEGF (100 µg mL^{-1})	3.06 (2.66-3.46)
EGF@Quatsomes (25 µg mL^{-1})	1.27 (0.87-1.67)
EGF@Quatsomes (100 µg mL^{-1})	1.40 (1.00-1.80)

Figure 3. In vitro studies of biological activity and proteolytic stability of EGF@Quatsomes. a) Specific biological activity of rhEGF and EGF@Quatsomes in cell proliferation assay in 3T3 A431 murine fibroblast cell line. b) Idealized scheme illustrating the potential mechanism of interaction of free rhEGF and EGF@Quatsomes with the EGF receptor at the cell surface, which seems more favorable for EGF@Quatsomes. c) Assessment of time-course proteolytic stability of free rhEGF at 25 and 100 µg mL^{-1} (red and purple lines, respectively) and EGF@Quatsomes at 25 and 100 µg mL^{-1} (gray and green lines, respectively) against chymotrypsin at 32 °C in the dispersant media (EtOH 10% v/v in 5 × 10^{-3} M histidine–HCl buffer, pH 7.0). d) Idealized scheme illustrating the potential protection of rhEGF from wound environment proteolytic degradation by its incorporation to quatsomes as compared to free protein. Inset Table shows a mean half-maximal effective dose (ED_{50}) and 95% confidence interval (CI) for the same groups. In a and c, data plotted as mean ± SD (n = 8 in a and n = 4 in c per group). In c, red, purple, grey, and green asterisk represents statistical significance for free rhEGF at 25 µg mL^{-1}, free rhEGF at 100 µg mL^{-1}, EGF@Quatsomes at 25 µg mL^{-1}, and EGF@Quatsomes at 100 µg mL^{-1} experimental groups, respectively, at the indicated time point. *$p < 0.05$, **$p < 0.01$, ***$p < 0.001$ and NS: non-significant differences. All statistical analyses were conducted by one-way ANOVA followed by Tukey pairwise comparison. *p*-Values for specific bioactivity and ED50 are shown in Table S6, Supporting Information, and for remanent rhEGF by ELISA in Table S8, Supporting Information.

100 µg mL^{-1}. On the other hand, for EGF@Quatsomes incubated between 6 and 24 h, the amounts of protein remained practically constant near to 70% for EGF@Quatsomes at 25 µg mL^{-1} and near to 40% at 100 µg mL^{-1}. At the same rhEGF bulk concentration, the overall percentage of undamaged protein was about 35–50%; higher when it is nano-formulated in quatsomes than free. Likely, the free rhEGF degrades much quicker than the rhEGF grafted on quatsomes because the free protein will exhibit multiple degradation sites exposed to the solvent (Figure 3d). Solvent exposed active sites of the protein may be recognized by a broader array of degradative enzymes like proteases. Since the ultimate purpose of this work was the use of the EGF@Quatsomes as a topical formulation, a high resistance to proteases might be translated to better bioavailability and a longer and more effective action of the rhEGF in the wound's areas.

2.6. Biocidal Activity of EGF@Quatsomes

As already mentioned, wound infection is one of the most important factors that contribute to wound chronicity and, thereby, efficient control of infection is an appropriate quality attribute for a drug topical delivered intended to treat chronic wounds. Samples of EGF@Quatsomes with rhEGF concentrations of 25 and 100 µg mL^{-1} and Blank@Quatsomes were tested in vitro to evaluate their biocide activity (see Methods, Supporting Information, for details). The effectiveness of the different colloidal systems was assayed against bacteria, yeast, and fungus. As shown in **Figure 4**a,b, EGF@Quatsomes, as well as Blank@Quatsomes presented antimicrobial activity against gram-positive bacteria, yeast, and fungi (Figure S10, Supporting Information). Remarkable is the fact that some microorganisms sensitive to EGF@Quatsomes (e.g., *Staphylococcus aureus*) are among the main microorganisms known to contribute to serious complications in wound infection and microbial flora of chronic wound biofilms and burns.[30] The encountered antimicrobial properties of EGF@Quatsomes demonstrated the great potential of the preparations based on quatsomes as topical formulations. The antimicrobial activity of quaternary ammonium surfactants (QASs) has generally been assigned to their ability to destroy cell membrane structure.[31] Indeed, QASs exert antimicrobial activity through its positive charge at physiological pH, which destabilizes bacterial cell walls and alters bacterial osmotic equilibrium.[12] These events result in the precipitation of cytoplasmic contents and trigger microbial cell death.[32] By their antiseptic activity, EGF@Quatsomes may also act as a prophylactic agent that prevents microbial

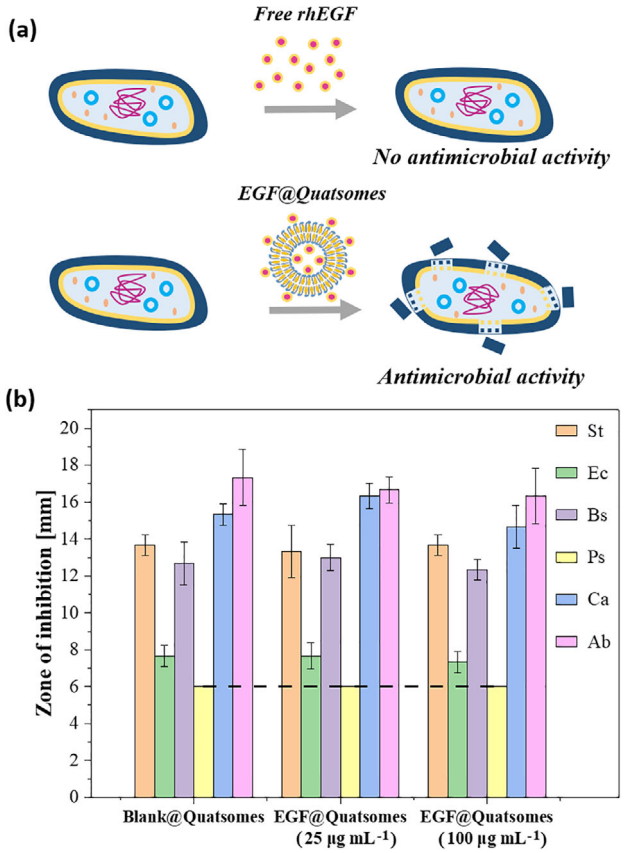

Figure 4. Antimicrobial activity of assayed quatsomes. a) Scheme illustrating the EGF@Quatsomes antimicrobial activity against potential wound environment microorganism. b) Antimicrobial activity assessed by a zone of inhibition during the agar well diffusion assays: Blank@Quatsomes and EGF@Quatsomes with rhEGF at 25 and 100 μg mL^{-1} bulk concentration against different microorganisms. St: *Staphylococcus aurous*; Ec: *Escherichia coli*; Bs: *Bacillus subtilis*; Ps: *Pseudomonas aeruginosa*; Ca: *Candida albicans*; Ab: *Aspergillus brasiliensis*. The discontinuous line represents the well diameter. In b, data plotted as mean ± SD ($n = 3$ per group).

infections, hindering the formation of biofilms. It has been already reported that Blank@Quatsomes have antibiofilm activity against *Staphylococcus aureus* and *Pseudomonas aeruginosa* biofilms.[33] According to these findings, the anchoring of rhEGF to nanovesicles could favor dimerization-dependent EGF–EGFR signaling while shielding the protein from other degradation pathways, permitting optimization of their pharmacological properties. Topical treatment with EGF@Quatsomes could also reduce the potential microorganism infections and protect the wound from further contaminations.

2.7. In Vitro Dermal Irritancy Tests of EGF@Quatsomes

The in vitro skin irritation test based on the OECD guideline 439 was performed with the human epidermal model EpiSkin (Episkin, Lyon)[34] to assess the skin tolerance of EGF@Quatsomes. To study the potential cytotoxicity of CTAB,[35] in addition to EGF@Quatsomes and Blank@Quatsomes, a solution of this cationic surfactant prepared in the same medium and at equivalent surfactant concentration as in the nanoconjugates was evaluated as a reference. Under the applied experimental conditions, results obtained on cell viability and interleukin-1α release (proinflammatory factor released in response to an irritant), after 24 and 48 h of product exposure, enabled to classify the quatsomes as "non-irritant" (Figures S11 and S12, Supporting Information). However, the CTAB solution induced an irritant response at both exposure times. In that case, cell viability was <50% and interleukin-1α release was >40 pg mL^{-1}, the latter value being similar to the one observed by the negative control of the experiment (solution of 5% SDS in PBS). Therefore, this in vitro test suggested that irritation induced by CTAB is widely reduced when nanostructured in quatsomes, indicating that EGF@Quatsomes could be well tolerated by the topical route.

2.8. Ex Vivo Permeation of EGF@Quatsomes in Human Skin

To evaluate the kinetics and absorption profile of the rhEGF contained in the EGF@Quatsomes through the skin, permeation assays in Franz-type diffusion cells were performed. Human skin with the barrier function impaired by tape-stripping was used to better reproduce the permeation behavior in wounds. As a reference, a solution of free rhEGF was evaluated using the same medium and containing an equivalent total rhEGF quantity as carried in quatsomes. Permeation of rhEGF was significantly reduced when encapsulated in quatsomes (Figure S13a, Supporting Information). rhEGF flux in the linear part of the curve showed that permeation was 2.7 times slower in EGF@Quatsomes than in the free rhEGF solution, being of 123 and 330 ng cm^{-2} h^{-1}, respectively. After 24 h, rhEGF contained in the free rhEGF solution permeated completely (103% ± 28%), while only half of the dose of the encapsulated rhEGF trespassed the skin (50% ± 10%) (Figure S13b, Supporting Information). This result suggests that the encapsulation of rhEGF in quatsomes allows better retention of the protein in the skin, achieving a more local and durable effect and, consequently, a more effective and efficient treatment. Also, quantification of CTAB after 24 h showed that only 5% of the applied dose permeated, which minimizes the safety concerns of using this cationic surfactant (Figure S13c, Supporting Information).

2.9. Wound Healing Efficacy of EGF@Quatsomes in a Diabetic Mouse Model

The main objective of this study was to evaluate wound healing capacity (ulcer reduction) of EGF@Quatsomes applied to excisional wounds in genetically db/db diabetic mice by the topical route. Treatment was administered locally in the wound area by using a sterile drip micropipette, and the wound was subsequently covered with a sterile semi-permeable dressing Tegaderm as described in the Materials and Methods section of the Supporting Information. Indeed, during a treatment applied three times a week for 14 days an increase in the closing speed of the wound was observed for the mice group treated with EGF@Quatsomes (rhEGF 100 μg mL^{-1}) and free rhEGF 100 μg mL^{-1} in the dispersant media compared with those groups treated with Blank@Quatsomes and only with the dispersant media (**Figure 5**a). Comparing with Blank@Quatsomes

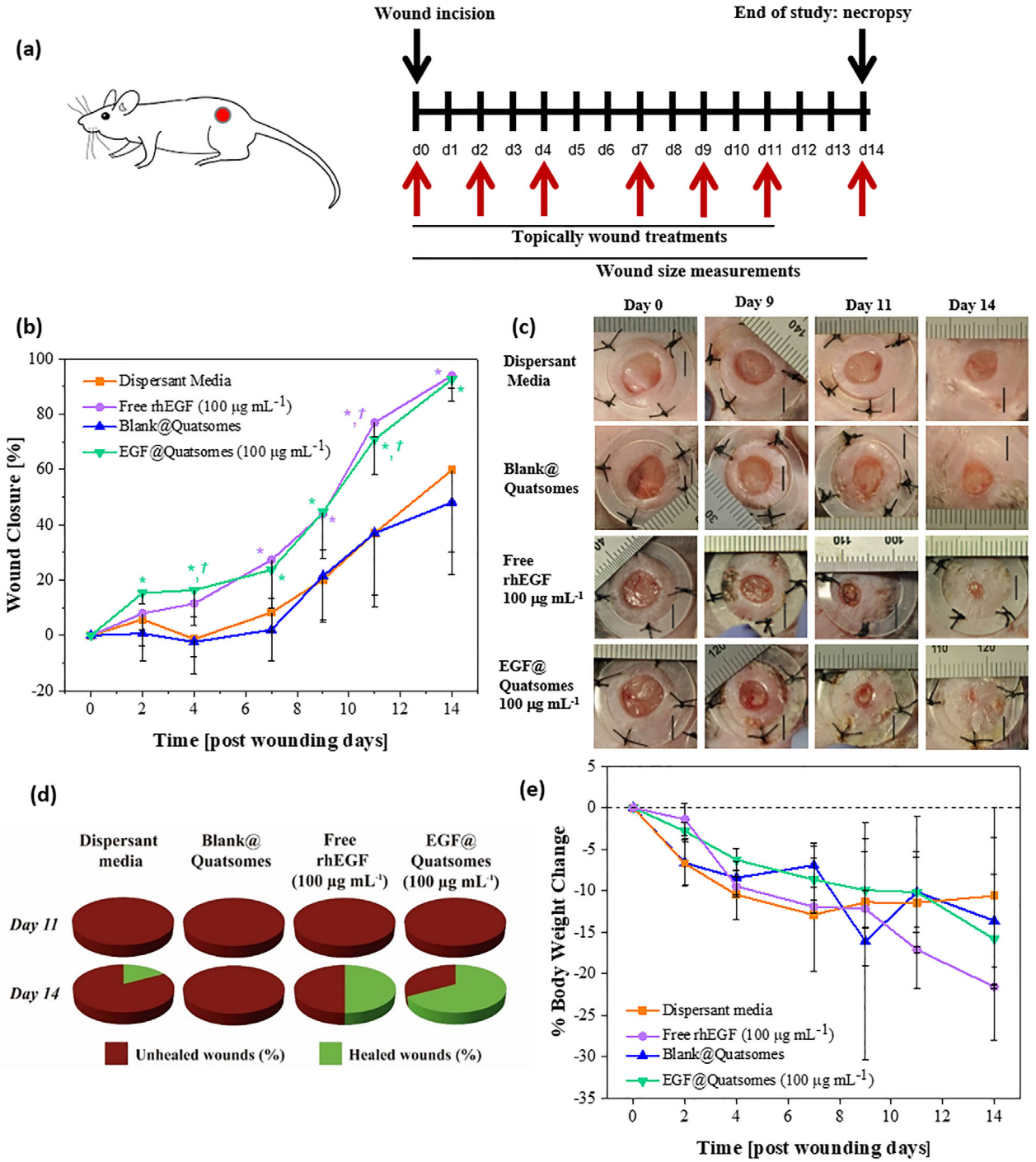

Figure 5. In vivo wound healing efficacy and toxicity study in db/db mice. Pharmacological evaluation of EGF@Quatsomes in cutaneous wound model in db/db mice. a) Overview of study design. b) The closing speed of EGF@Quatsomes (rhEGF 100 µg mL^{-1}) (green triangles), Blank@Quatsomes (blue triangles), dispersant media (orange squares), and free rhEGF 100 µg mL^{-1} (purple dots). c) Representative photograph during the topical treatment following of the wound healing process in the groups. Bar represents 5 mm. d) Evolution of healed wounds of different groups after 11 and 14 days of treatment. Wounds were considered healed only when more than 95% of wound closure was achieved. e) The evolution of body weight of all animals was recorded during each treatment with EGF@Quatsomes (green triangles), Blank@Quatsomes (blue triangles), dispersant media (orange squares), and free rhEGF (purple dots). All animals spearing healthy throughout the study based on eating and behavior under their condition of hyperglycemic. In b and e, data plotted as mean ± SD. The number of animals werewas $n = 3$ (two wounds per animal) except for the free rhEGF group with $n = 2$. In b, *significant differences with respect to the Blank@Quatsomes group, and †significant differences with respect to the dispersant media group. $^{*,\dagger}p < 0.05$ (*,†EGF@Quatsomes group, and *,†free rhEGF group),). In e, no statistical differences for body weight change among treated animal groups. All statistical analyses were by one-way ANOVA followed by Tukey pairwise comparison. P-values for wound closure are shown in Table S9, Supporting Informatio, and for body weight in Table S11, Supporting Information.

statistically significant differences in percent wound closure were observed in favor of the EGF@Quatsomes since day 2 onwards of treatment while for free rhEGF, the differences start from day 7 onwards of treatment. Furthermore, comparing with dispersant media statistically significant differences in percent wound closure were observed in favor of the EGF@Quatsomes at days 4 and 11 of treatment while for free rhEGF the differences were only at day 11 of treatment (Figure 5b; Table S9, Supporting Information). On the other hand, compared to the baseline area of the wound at day 0, statistically significant differences were observed from day 7 onwards of treatment for the EGF@Quatsomes group and day 9 onwards of treatment with free rhEGF, while for Blank@Quatsomes and dispersant media groups the differences start from day 11 onwards (Figure S14a and Table S10, Supporting Information). So, earlier statistical differences in percent wound closure compared to control groups and of wound area compared to the baseline at day 0 were observed for EGF@Quatsomes in comparison to free rhEGF. Moreover, the baseline wound area at day 0 was statistically significant larger for the group treated with EGF@Quatsomes compared to the group treated with free rhEGF in the dispersant media ($p = 0.013$).

Interestingly, the closing speed of the wound with the first doses of EGF@Quatsomes was somewhat superior to the free rhEGF although this difference was equilibrated at later dosing probably because of the high concentration of rhEGF used in this assay, which may compensate for the higher efficacy of EGF@Quatsomes. Representative photography images of wound evolution at days 0, 9, 11, and 14 of treatment clearly show the faster speed of closing wound in the EGF@Quatsomes group with respect to the controls (Figure 5c). Because the current clinical practice demands a complete closure of the wound and not the partial reduction of the wound area, the percentage of closed wounds in the different groups was also evaluated, considering that wound healing occurs only when the closure was greater than 95%. Under this criterion, after 11 days of treatment, any group showed all wounds healed. However, the percentage of wound closure was 67% at 14 days of study for the EGF@Quatsomes group, while for the control Blank@Quatsomes, dispersant medium, and free rhEGF control groups were 0%, 17%, and 50%, respectively (Figure 5d).

After the wound healing study, the most relevant clinical symptomatology for all mice was evaluated. All animal groups show high levels of glucose (hyperglycemia) during the treatment (about 600 mg dL^{-1}), compared to normal levels of the species (about 200 mg dL^{-1}), in agreement with the pathology of the animals, i.e., their diabetic condition, and no statistically significant difference (ANOVA p-value = 0.289) were observed among groups (Figure S14b, Supporting Information). Because bodyweight change is considered critical for safety evaluation, this was monitored during the study. As shown in Figure 5e, in all treatment groups, a decrease in body weight was observed during the study, but no statistical differences were observed among the four groups at any time measured during the 14 days treatment period (Table S11, Supporting Information). The decrease in body weight was supposed to be associated with the conditions of animals, hyperglycemic and obese mice with large wounds, and not causally related to the EGF@Quatsomes treatment. Furthermore, no further toxicity signs were associated with the EGF@Quatsomes treatment considering clinical symptoms, hematological, and biochemical evaluations with no statistically significant differences among the study groups in none of the parameters (Table S12, Supporting Information).

2.10. Topical Treatment with EGF@Quatsomes in DFU Patients

Taking into account the previous in vitro and animal model outcomes with EGF@Quatsomes, the EGF@Quatsomes effectiveness (rhEGF 100 μg mL^{-1}) upon its topical administration was examined in a small cohort of chronic diabetic feet ulcer (DFU) affected patients. Although most of the wounds were predominantly classified as neuropathic (80%), all exhibited long-term evolution data giving their refractoriness to contraction and re-epithelialization. At a primary microscopic assessment, the granulation tissue exhibited signs of senescence and fibrosis. Accordingly, the hypothesis that this intervention could significantly assist in reverting the evolved chronic phenotype was accrued. Patient demographics and ulcer characteristics are illustrated in Table S13, Supporting Information. As shown, the male gender (80%) and adults over 50 (52–69 years old) predominated. Wounds size (2.4–26 cm^2), evolution time (5–60 months), and location were variable. Nevertheless, chronicity evolvement represents an unusual and impressive profile, which entails a poor prognostic. None of the patients treated with EGF@Quatsomes suspension discontinued the treatment because of ulcer infection, inflammation, or any other phlogistic sign. EGF@Quatsomes intervention proved to be safe and well-tolerated. The wounds were treated in an out-patient regime. Accordingly, they were cleansed, surgically debrided, treated with the EGF@Quatsomes, and dressed with a sterile gauze every Monday, Wednesday, and Friday at the diabetic angiopathy ward of the National Institute of Angiology, Havana, Cuba. The wound surface area (WSA) of patients was measured weekly and the kinetic evolution of wound area was plotted for each of the five treated patients (**Figure 6**a). The three times per week EGF@Quatsomes suspension treatment accounted for a significant closure response in ≈90 days. In the 12th week, three out of five patients had full re-epithelialization of the wounds. The remaining patient exhibited a growing productive granulation tissue with an area reduction larger than 80% in which contraction and re-epithelialization were observed (Figure 6a,b; Figure S15, Supporting Information). Irrespective of the lack of a concurrent control group, this result is encouraging given the steady epithelial response shown by the patients within a shorter temporary window as compared to other studies with better prognostic wounds.[36] As judged by our observations, the EGF@Quatsomes established a significant clinical improvement from week 4 onward, thus establishing a sort of phenotypic turning point. Small biopsies collected at the end of the fourth week for histological and immunohistochemical characterization indicated the activation of the EGFR signaling axis, given the positive immunolabeling to the EGFR and the downstream PI3K and AKT transducers. Of note, phosphorylations were detected for all tyrosine catalytic residues when compared to paired pre-treatment fragments (Figure 6c). This modality of EGF delivery entails a meaningful therapeutic achievement, considering the protracted evolution of the targeted wounds and the complexity of the molecular mechanisms behind the onset and perpetuation of diabetic

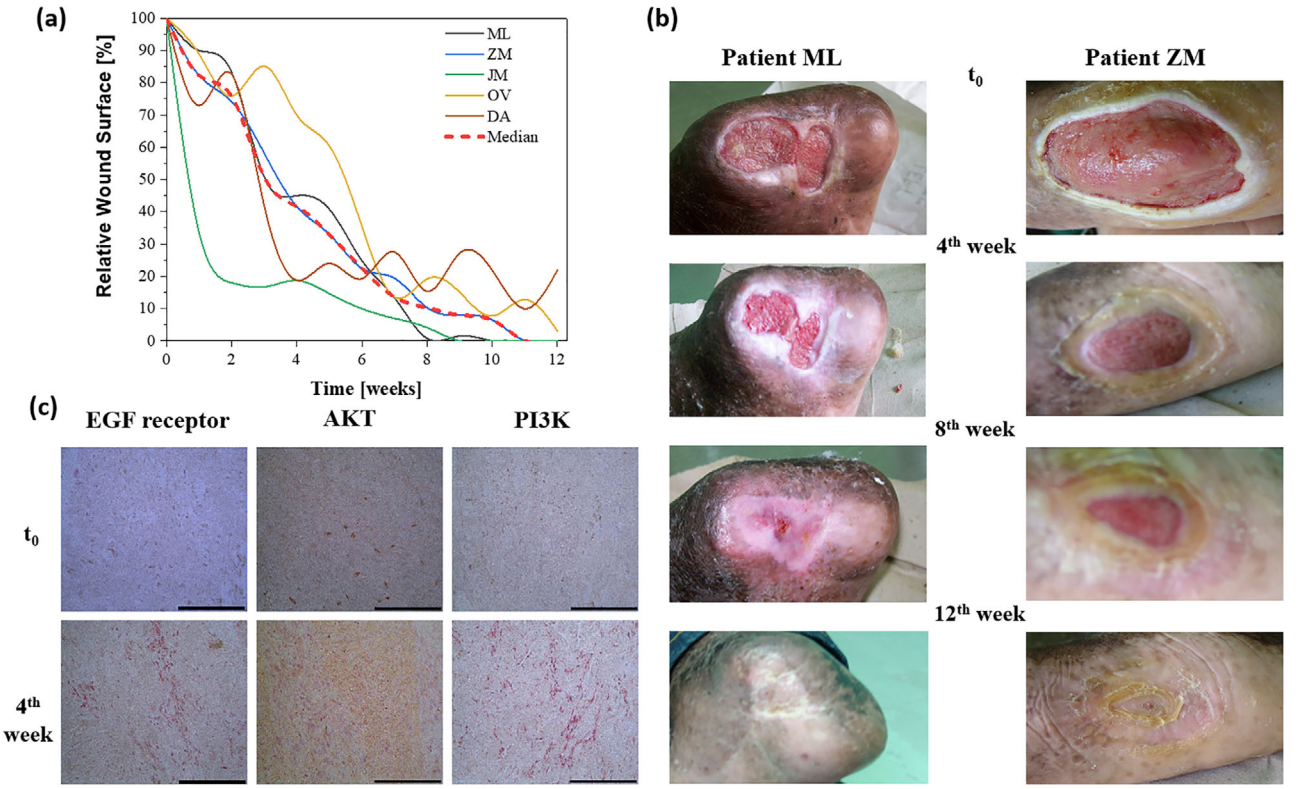

Figure 6. A compassionate case study in patients with DFU. Suspensions of EGF@Quatsomes at 100 μg mL^{-1} rhEGF were irrigated over the lesion and its borders. a) Reduction of wound surface area values of DFU during the time course of 12 weeks with EGF@Quatsome suspension plus good wound care treatment of five patients, also shown the median. b) Images showing the time course of wound healing in patients ML and ZM after 0th, 4th, 8th, and 12th weeks they received the EGF@Quatsome treatment. c) Histological sections of patient ZM biopsies were stained by immunohistochemistry with the anti-EGFR, AKT, and PI3 antibodies and were counterstained with Haematoxylin (magnification 40×) bar represents 100 μm.

wounds' chronicity.[37] In conclusion, the topical application of EGF@Quatsomes offers a broad pharmacodynamic potential, in addition, to being safe and well-tolerated.

3. Conclusion

Novel nanoconjugates based on nanovesicles, named quatsomes and formed by cholesterol and CTAB containing recombinant human EGF (EGF@Quatsomes), have been prepared using the DELOS-susp manufacturing platform with compressed CO_2. The resulting EGF@Quatsomes, loaded with 25 and 100 μg mL^{-1} of protein, showed appropriate values of the major critical quality attributes of colloidal nanomedicines, which play important roles in determining their stability, drug loading, drug protection, targeting ability, and bioactivity. Indeed, these nanoconjugates exhibit homogeneous spherical morphologies with nanoscopic sizes (mean hydrodynamic diameters of ≈60 nm and PDI of ≈0.3), highly positive charged surfaces (apparent zeta potentials above +70 mV), and unilamelarities together with large stability overtime for more than 90 weeks under storage conditions. Moreover, such nanoconjugates do not show any rhEGF release when stored at pH 5.5 and 37 °C after 3 days. They were obtained with a very high EE% (≥97%) and with a complete reproducibility of their physicochemical characteristics from bench-scale to pilot-scale. The rhEGF protein is grafted by electrostatic interactions on the nanovesicle' membrane together with a contribution of hydrogen bonding or protein reorganization, and these interactions do not alter significantly the secondary and higher-order structures of the protein. Such multiple supramolecular interactions are responsible for the dissociation constant of the rhEGF of EGF@Quatsome conjugates higher than that of free rhEGF and cellular EGFRs, making quatsomes an appropriate nanocarrier for the transportation of the protein towards its target without compromising the ultimate interaction of the protein with its receptor. In vitro protein-specific bioactivity of EGF@Quatsomes, measured by cell proliferation with mouse fibroblasts, was not only preserved but increased at least twice with respect to the free rhEGF, without exhibiting significant cytotoxicity. This effect is attributed to the immobilization of the protein in the vesicle membrane with probably a site-specific orientation of the active protein region towards the surrounding media and possibly also to a nanometric scale clustering of protein active sites on the quatsomes that could favor multimerization of the receptor. Integration of rhEGF in the vesicle membranes not only increases cell proliferation activity but also preserves the protein stability in the presence of a protease model, like chymotrypsin, since the percentage of undamaged rhEGF protein after incubation during 24 h was about 40–70% in comparison of 5–20% attained for free rhEGF. Another significant advantage of EGF@Quatsomes is their biocidal activity, against Gram-positive bacteria, yeast, and fungus, produced by the presence of the quaternary ammonium surfactant in the nanovesicle composition. This surfac-

tant exerts antimicrobial activity through its positive charge at the physiological pH which destabilizes bacterial cell walls. This antiseptic activity of EGF@Quatsomes may act as a prophylactic agent preventing microbial infections hindering the formation of biofilms being therefore attractive for topical treatments. EGF@Quatsomes can be classified as a skin non-irritant system according to in vitro assay with human epidermal EpiSkin model analyzing cell viability and interleukine-1α release, as a marker of irritant processes. Ex vivo permeation tests with the EGF@Quatsomes, using impaired human skin and a Franz-type cell, did not show an effective permeation of rhEGF through the skin suggesting its inability to reach the circulation system when topically administered. Evaluation of wound healing capacity, through ulcer reduction assessment, of EGF@Quatsomes was also performed. These assays indicated that when applied by a topical route on excisional wounds artificially produced in genetically diabetic mice a 67% of mice presented a complete wound closure after 14 days without any sign of toxicity while assays with proper controls only showed 0–50% wound closures. Furthermore, the closing speed of the wound with the first doses of EGF@Quatsomes was clearly superior to the control free rhEGF. Due to the successful in vitro and animal results obtained with EGF@Quatsomes, the topical effectiveness of this drug delivery system was evaluated in five compassionate patients with DFUs with different wound sizes, ulcer duration, and location. A thrice-weekly treatment of chronic DFU with irrigation of an EGF@Quatsome dispersion on the ulcers, plus good wound care (GWC), significantly increased the incidence of complete and higher than 80% healing. At the end of the study (12 weeks), three out of five patients had full re-epithelialization of the wounds and the rest showed a reduction in wound size higher than 80% with only mild-to-moderate side-effects. Remarkably, non patient exhibited incidence of wound infection-related adverse events associated with the ulcer. Moreover, no further toxicity signs were associated with the EGF@Quatsomes treatment considering clinical symptoms, hematological, and biochemical evaluations.

It is worth mentioning that due to its molecular composition and supramolecular structure, EGF@Quatsomes have a dual therapeutic action preventing the infection and promoting the regeneration of granulation tissue and re-epithelialization of complex wounds such as DFUs. Furthermore, such nanoconjugates fulfill the basic requirements, related to their production, storage stability, patient compliance, and high efficacy with minimal side effects, to be considered as a potential nanomedicine to enter in future clinical assays for the treatment of DFUs and presumably of VLUs and PUs.

4. Experimental Section

Materials and experimental details are provided in the Supporting Information.

All animal experiments were approved by the Committee on the Ethics of Animal Experiments of Minimally Invasive Surgery Centre Jesús Usón and by the Council of Agriculture and Rural Development of the Regional Government of Extremadura (APAFIS#4438-2015092514508030 v7), and in accordance with the INSERM guidelines and European Community directives for the care and use of laboratory animals (Cáceres, Spain).

Five adult patients were recruited at the Angiopathy ward service of the hospital National Institute for Angiology and Vascular Surgery (INACV, La Habana, Cuba). The study was carried out in accordance with relevant institutional and national guidelines, and the protocol was approved by the Ethics committee of the hospital National Institute for Angiology and Vascular Surgery (INACV, La Habana, Cuba). The principles of the World Medical Association's Declaration of Helsinki were followed. The patients gave written informed consent to participate in the study and for publication of the data.

Supporting Information

Supporting Information is available from the Wiley Online Library or from the author.

Acknowledgements

L.F.-T and H.S. contributed equally to this work. This work was funded by the Spanish Ministry/FEDER project MOTHER MAT2016–80826-R; the Networking Research Center on Bioengineering, Biomaterials, and Nanomedicine (CIBER-BBN); the Generalitat de Catalunya (2017SGR918); and the Spanish Ministry of Economy and Competitiveness by the Severo Ochoa FUNFUTURE (CEX2019-000917-S) Excellence Centre distinction. This work was also co-financed by the European Union through FEDER project NANONAFRES (COMRDI15-1-0023). The authors thank Milagros Font and Yenay Diaz from CIGB for technical assistance. The authors also thank the Industrial Doctorates Plan of Agaur-Generalitat de Catalunya (2018 DI 057). Some figures of this work were created using Servier Medical Art templates, which are licensed under a Creative Commons Attribution 3.0 Unported License.

Conflict of Interest

The authors declare the following financial interests/personal relationships which may be considered as potential competing interests: L.F.-T., E.G.-M., L.B.-H., C.C.-A., A.C., J.M-M., H.G., G.C.,V.F., E.M.-C., J.S.P., J.R., C.N.-R., C.V., M.L., and S.S. declare no conflict of interest. H.S., I.C.-P, J.B., E.M., J.V., and N.V. are the inventors of patent WO/2014/019555 licensed to Heber Biotec S.L. S.S., J.V., and N.V. are the inventors of patent WO/2006/079889, owned by Nanomol Technologies SL, and have stock ownerships at Nanomol Technologies SL.

Data Availability Statement

Research data are not shared.

Keywords

chronic wounds, nanomedicine, nanovesicles, rhEGF, therapy

Received: November 16, 2020
Revised: February 13, 2021
Published online: March 12, 2021

[1] a) C. K. Sen, G. M. Gordillo, S. Roy, R. Kirsner, L. Lambert, T. K. Hunt, F. Gottrup, G. C. Gurtner, M. T. Longaker, *Wound Repair Regener.* **2009**, *17*, 763; b) V. W. Wong, G. C. Gurtner, *Exp. Dermatol.* **2012**, *21*, 729.
[2] R. F. Diegelmann, M. C. Evans, *Front. Biosci.* **2004**, *9*, 283.
[3] D. G. Armstrong, J. Wrobel, J. M. Robbins, *Int. Wound J.* **2007**, *4*, 286.
[4] D. F. Bandyk, *Semin. Vasc. Surg.* **2018**, *31*, 43.
[5] G. C. Gurtner, S. Werner, Y. Barrandon, M. T. Longaker, *Nature* **2018**, *453*, 314.

[6] N. X. Landén, D. Li, M. Ståhle, *Cell. Mol. Life Sci.* **2016**, *73*, 3861.
[7] A. J. Boulton, D. G. Armstrong, M. J. Hardman, M. Malone, J. M. Embil, C. E. Attinger, R. S. Kirsner, in *Diagnosis and Management of Diabetic Foot Infections*, American Diabetes Association, Arlington, VA **2020**. https://doi.org/10.2337/db2020-01.
[8] N. Škalko-Basnet, *Biol.: Targets Ther.* **2014**, *8*, 107.
[9] J. Berlanga-Acosta, Y. Mendoza-Mari, A. Garcia-Ojalvo, M. Fernandez-Mayola, G. Guillen-Nieto, *J. Diabetes Metab.* **2018**, *9*, 1000798.
[10] S. Hamdan, I. Pastar, S. Drakulich, E. Dikici, M. Tomic-Canic, S. Deo, S. Daunert, *ACS Cent. Sci.* **2017**, *3*, 163.
[11] V. W. Wong, G. C. Gurtner, *Exp. Dermatol.* **2012**, *21*, 729.
[12] S. Barrientos, O. Stojadinovic, M. S. Golinko, H. Brem, M. Tomic-Canic, *Wound Repair Regener.* **2008**, *16*, 585.
[13] P. A. Lopez-Saura, J. Berlanga-Acosta, C. Valenzuela-Silva, O. Gonzalez-Diaz, W. Savigne, B. Acevedo-Castro, in *Global Perspective on Diabetic Foot Ulcerations* (Ed: T. Dinh), IntechOpen, London**2011**, pp. 217–238.
[14] S. Hamdan, I. Pastar, S. Drakulich, E. Dikici, M. Tomic-Canic, S. Deo, S. Daunert, *ACS Cent. Sci.* **2017**, *3*, 163.
[15] I. Tocco, B. Zavan, F. Bassetto, V. Vindigni, *J. Nanomater.* **2012**, *2012*, 714134.
[16] a) L. Ferrer-Tasies, E. Moreno-Calvo, M. Cano-Sarabia, M. Aguilella-Arzo, A. Angelova, S. Lesieur, S. Ricart, J. Faraudo, N. Ventosa, J. Veciana, *Langmuir* **2013**, *29*, 6519; b) N. Grimaldi, F. Andrade, N. Segovia, L. Ferrer-Tasies, S. Sala, J. Veciana, N. Ventosa, *Chem. Soc. Rev.* **2016**, *45*, 6520; c) H. Santana, N. Ventosa, E. Martinez, J. Berlanga, I. Cabrera, J. Veciana, *WO2014/019555*, **2012**.
[17] S. Quirce, P. Barranco, *J. Invest. Allergol. Clin. Immunol.* **2010**, *20*, 542.
[18] a) P. L. Tran, E. Huynh, A. N. Hamood, A. de Souza, G. Schultz, B. Liesenfeld, D. Mehta, D. Webster, T. W. Reid, *Int. Wound J.* **2017**, *14*, 79; b) X. Ye, J. Feng, J. Zhang, X. Yang, X. Liao, Q. Shi, S. Tan, *Colloids Surf. B* **2017**, *149*, 322.
[19] a) M. Cano-Sarabia, N. Ventosa, S. Sala, C. Patiño, R. Arranz, J. Veciana, *Langmuir* **2008**, *24*, 2433; b) I. Cabrera, E. Elizondo, O. Esteban, J. L. Corchero, M. Melgarejo, D. Pulido, A. Córdoba, E. Moreno, U. Unzueta, E. Vazquez, I. Abasolo, S. Schwartz, Jr., A. Villaverde, F. Albericio, M. Royo, M. F. García-Parajo, N. Ventosa, J. Veciana, *Nano Lett.* **2013**, *13*, 3766; c) I. Cabrera, I. Abasolo, J. L. Corchero, E. Elizondo, P. Rivera-Gil, E, M., J. Faraudo, S. Sala, D. Bueno, E. González-Mira, M. Rivas, M. Melgarejo, D. Pulido, F. Albericio, M. Royo, A. Villaverde, M. F. García-Parajo, S. Schwartz, Jr., N. Ventosa, J. Veciana, *Adv. Healthcare Mater.* **2016**, *5*, 829; d) M. A. W. Eaton, *J. Control. Release.* **2012**, *164*, 370.
[20] A. Porfire, M. Achim, C. Barbalata, I. Rus, I. Tomuță, C. Cristea, in *Pharmaceutical Development of Liposomes Using the QbD Approach*, IntechOpen, London**2019**, Ch. 2. https://doi.org/10.5772/intechopen.85374.
[21] T. Narayanan, J. Gummel, M. Gradzielski, in *Advances in Planar Lipid Bilayers and Liposomes*, Vol. 20 (Eds: A. Iglič, C. V. Kulkarni), Academic Press, San Diego, CA**2014**, Ch. 7.
[22] A. Ali, Shahjahan, *Z. Phys. Chem.* **2008**, *222*, 1519.
[23] A. Bonvicini, L. Guilhaudis, V. Tognetti, D. Desmaële, N. Sauvonnet, H. Oulyadi, L. Joubert, *Phys. Chem. Chem. Phys.* **2018**, *20*, 5274.
[24] H. W. Huang, S. K. Mohan, C. Yu, *Biochem. Biophys. Res. Commun.* **2010**, *402*, 705.
[25] J. Seelig, *Biochim. Biophys. Acta, Biomembr.* **2004**, *1666*, 40.
[26] S. R. Feroz, S. N. A. Malek, S. Tayyab, *Braz. J. Pharm. Sci.* **2016**, *52*, 443.
[27] J. M. Sanders, M. E. Wampole, M. L. Thakur, E. Wickstrom, *PLoS One* **2013**, *8*, e54136.
[28] a) A. R. Mire-Sluis, T. Gerrard, R. G. Das, A. Padilla, R. Thorpe, *Biologicals* **1996**, *24*, 351; b) P. P. Di Fiore, J. H. Pierce, T. P. Fleming, R. Hazan, A. Ullrich, C. R. King, J. Schlessinger, S. A. Aaronson, *Cell* **1987**, *51*, 1063.
[29] A. Abulrob, Z. Lu, E. Baumann, D. Vobornik, R. Taylor, D. Stanimirovic, L. J. Johnston, *J. Biol. Chem.* **2010**, *285*, 3145.
[30] B. A. Lipsky, C. Hoey, *Clin. Infect. Dis.* **2009**, *49*, 1541.
[31] Y. Jiao, L. Niu, S. Ma, J. Li, F. R. Tay, J. Chen, *Prog. Polym. Sci.* **2017**, *71*, 53.
[32] B. A. Mast, G. S. Schultz, *Wound Repair Regener.* **1996**, *4*, 411.
[33] a) N. Thomas, D. Dong, K. Richter, M. Ramezanpour, S. Vreugde, B. Thierry, P. J. Wormald, C. A. Prestidge, *J. Mater. Chem. B* **2015**, *3*, 2770; b) D. Dong, N. Thomas, M. Ramezanpour, A. J. Psaltis, S. Huang, Y. Zhao, B. Thierry, P. J. Wormald, C. A. Prestidge, S. Vreugde, *Exp. Biol. Med.* **2020**, *245*, 34.
[34] OECD, *Test No. 439: In Vitro Skin Irritation: Reconstructed Human Epidermis Test Method*, OECD Publishing, Paris **2015**.
[35] a) C. Gloxhuber, *Arch. Toxicol.* **1974**, *32*, 245; b) R. C. Rowe, P. J. Sheskey, M. E. Quinn, *Handbook of Pharmaceutical Excipients*, 6th ed., Pharmaceutical Press, London **2009**.
[36] a) C. R. Waycaster, A. M. Gilligan, T. A. Motley, *J. Am. Podiatr. Med. Assoc.* **2016**, *106*, 273; b) J. M. Smiell, T. J. Wieman, D. L. Steed, B. H. Perry, A. R. Sampson, B. H. Schwab, *Wound Repair Regener.* **1999**, *7*, 335; c) K. H. Park, S. H. Han, J. P. Hong, S. K. Han, D. H. Lee, B. S. Kim, J. H. Ahn, J. W. Lee, *Diabetes Res. Clin. Pract.* **2018**, *142*, 335.
[37] D. G. Armstrong, A. J. Boulton, S. A. Bus, *N. Engl. J. Med.* **2017**, *376*, 2367.